The Astrophysical Journal, 629:615–624, 2005 August 20

THE NUMBER OF SUPERNOVAE FROM PRIMORDIAL STARS IN THE UNIVERSE

John H. Wise and Tom Abel
Kavli Institute for Particle Astrophysics and Cosmology, Stanford Linear Accelerator Center, 2575 Sand Hill Road, MS 29, Menlo Park, CA 94025; jwise@slac.stanford.edu, tabel@slac.stanford.edu
Received 2004 November 18; accepted 2005 March 23

ABSTRACT

Recent simulations of the formation of the first luminous objects in the universe predict isolated very massive stars to form in dark matter halos with virial temperatures large enough to allow significant amounts of molecular hydrogen to form. We construct a semianalytic model based on Press-Schechter formalism and calibrate the minimum halo mass that may form a primordial star with the results from extensive adaptive mesh refinement simulations. The model also includes star formation in objects with virial temperatures in excess of 10,000 K. The free parameters are tuned to match the optical depth measurements by the *WMAP* satellite. The models explicitly include the negative feedback of the destruction of molecular hydrogen by a soft UV background that is computed self-consistently. We predict high-redshift supernova rates as one of the most promising tools to test the current scenario of primordial star formation. The supernova rate from primordial stars peaks at redshifts of $\sim$20. Using an analytic model for the luminosities of pair-instability supernovae, we predict observable magnitudes and discuss possible observational strategies. Such supernovae would release enough metals corresponding to a uniform enrichment to a few hundred thousand solar. If some of these stars produce gamma-ray bursts, our rates will be directly applicable to understanding the anticipated results from the *Swift* satellite. This study highlights the great potential of the *James Webb Space Telescope* in probing cosmic structure at redshifts greater than 15.

Subject headings: cosmology: theory — early universe — supernovae: general

Online material: color figures

1. INTRODUCTION

The properties of pre-reionization luminous objects are integral to our comprehension of the process of reionization and their effect on subsequent structure formation. Observations of distant ($z = 6.28$, 6.4) quasars depict the relics of reionization with their accompanying Gunn-Peterson troughs (Becker et al. 2001; Fan et al. 2002). Furthermore, Lyα forest carbon abundances of $\sim 10^{-2}$ and $10^{-3.7}\ Z_\odot$ observed at redshifts of 3 and 5, respectively, indicate that numerous early supernovae (SNe) enriched the intergalactic medium (IGM; Songaila & Cowie 1996; Songaila 2001). These early generations of stars are at least partly responsible for ionizing the universe. A fraction of these stars lie in protogalaxies, but the other fraction of early stars are metal-free, form through molecular hydrogen cooling, and are very massive ($M \sim 100\ M_\odot$; Abel et al. 2000, 2002). In ΛCDM cosmologies, these stars form at $10 \lesssim z \lesssim 50$. The *Wilkinson Microwave Anisotropy Probe* (*WMAP*) data further constrain the epoch of reionization from the measurement of the optical depth due to electron scattering, $\tau_{\rm es} = 0.17 \pm 0.04$ (68% confidence), which corresponds to a reionization redshift of 17 ± 5 when assuming instantaneous reionization (Kogut et al. 2003). However, in this paper we show that this epoch is gradual and its effect on primordial star formation.

In hierarchical models of structure formation, small objects merge to form more massive structures. Eventually, a fraction of halos are massive ($\sim 5 \times 10^5\ M_\odot$ at $z \sim 20$) enough to host cooling gas (Couchman & Rees 1986; Tegmark et al. 1997; Abel et al. 1998; Fuller & Couchman 2000). These halos do not cool through atomic line cooling since $T_{\rm vir} < 10^4$; however, primordial gas contains a trace of H_2. Free electrons allow H_2 to form, which acts as an effective coolant at several hundred degrees through rotational and vibrational transitions. H_2 is easily photodissociated by photons in the Lyman-Werner (LW) band, 11.26–13.6 eV (Field et al. 1966; Stecher & Williams 1967); thus H_2 can be destroyed by distant sources in a neutral universe. Primordial stars produce copious amounts of UV photons in the LW band, destroying the most effective cooling process at $z \sim 20$. This negative feedback from the UV background significantly inhibits the primordial star formation rate in the early universe by requiring a larger potential well for gas to condense. Many groups have explored the effects of a UV background on cooling and collapsing gas. First, Dekel & Rees (1987) discovered that H_2 can be dissociated from large distances. Then more quantitatively, Haiman et al. (1997) questioned how collapsing, homogeneous, spherical clouds are affected by a UV background. In more detail, Haiman et al. (2000) determined whether a gas cloud collapsed by comparing the cooling time with the current lifetime of the cloud, which was calculated in the presence of solving the spherically symmetric radiative transfer equation along with time-dependent H_2 cooling functions. However, these studies only considered spherically symmetric cases, while realistically these halos are overdensities within filaments. To combat this problem, Machacek et al. (2001) employed a three-dimensional Eulerian adaptive mesh refinement (AMR) simulation to determine quantitative effects of a UV background on gas condensation.

We consider lower mass stars to form in more massive halos that may fragment via atomic line cooling, as well as from the metal lines from the heavy elements expelled by earlier generations of stars. We use the prescription outlined in Haiman & Loeb (1997) to model the metal abundances and ionizing photon rates of these stars.

With infrared space observatories, such as the *Spitzer Space Telescope*, the *Primordial Explorer* (*PRIME*; Zheng et al. 2003), and the *James Webb Space Telescope* (*JWST*), sufficient sensitivity is available to detect the SNe from primordial stars. Although SN remnants are bright for short periods of time, they

may be the best chance to directly observe primordial stars due to their large intrinsic luminosities. If these events are recorded, many properties, such as mass, luminosity, metallicity, and redshift, of the progenitors can be calculated using metal-free or ultra–metal-poor SN models, which can validate or falsify simulations of the first stars (Abel et al. 2002). To evolve our calculation through redshift, we need to retain information about the UV background and number densities of primordial stars, which can extend to determining such quantities as volume-averaged metallicity and ionized fraction of the universe. Our model is constrained by (1) the *WMAP* optical depth measurement, (2) primordial star formation and suppression in high-resolution hydrodynamic simulations, and (3) local observations of dwarf galaxies that constrain the properties of high-redshift protogalaxies.

We organize the paper as follows. In § 2 we report on the semi-empirical method behind our calculations, which incorporates effects from negative feedback and an ionized fraction and is constrained by the *WMAP* result and local dwarf galaxy observations. In § 3 we present the number density of primordial SNe in the sky. We also explore the feasibility of observing these SNe by calculating their magnitudes and comparing them with the sensitivities of infrared space observatories. Then in § 4 we discuss possible future observations and numerical simulations that could further constrain our model. Finally, § 5 summarizes our results and the implications of the first observations of SNe from primordial stars.

2. THE METHOD

We use several theories and results from simulations of structure formation and metal-free stars. We use a ΛCDM cosmology with $\Omega_\Lambda = 0.70$, $\Omega_{\rm CDM} = 0.26$, $\Omega_b = 0.04$, $h = 0.7$, $\sigma_8 = 0.9$, and $n = 1$. Here Ω_Λ, $\Omega_{\rm CDM}$, and Ω_b are the fractions of mass-energy contained in vacuum energy, cold dark matter, and baryons, respectively; h is the Hubble parameter in units of 100 km s^{-1} Mpc^{-1}; $n = 1$ indicates that we use a scale-free power spectrum; and σ_8 is the variance of random mass fluctuations in a sphere of radius 8 h^{-1} Mpc. We use a CDM power spectrum defined in Bardeen et al. (1986), which depends on σ_8 and h.

The remaining parameters are the primordial stellar mass and the factors $f_{\rm esc}$ and $f_\star$, which dictate the production and escape of ionizing photons; $f_{\rm esc}$ is the photon escape fraction, and $f_\star$ is the star formation efficiency.

To evolve the ionization and star formation behaviors of the universe, we must determine the density of dark matter halos that host early stars. In $T_{\rm vir} < 10^4$ K halos (henceforth "minihalos"), H_2 cooling is the primary mechanism that provides means of condensation into cold, dense objects. However, in $T_{\rm vir} > 10^4$ K, which corresponds to $M_{\rm vir} > 10^8\ M_\odot\ [(1+z)/10]^{-3/2}$ halos, hydrogen atomic line cooling allows the baryons to fragment and cool into stars.

2.1. *Minihalo Star Formation*

The first quantity we need to begin our calculation is the minimum halo mass that forms a cold, dense gas core due to H_2 cooling. Radiation in the LW band photodissociates H_2, which inhibits star formation in minihalos. This negative feedback from a UV background does not necessarily prohibit the formation of primordial stars in minihalos, but only increases the critical halo mass in which condensation occurs, and delays the star formation. From their simulations of pregalactic structure formation, Machacek et al. (2001) determined that the minimum mass of a halo that hosts a massive primordial star is

$$\frac{M_{\rm min}}{M_\odot} = \exp\left(\frac{f_{\rm cd}}{0.06}\right)\left(1.25\times10^5 + 8.7\times10^5 F_{\rm LW,-21}^{0.47}\right), \quad (1)$$

where $M_{\rm min}$ is the minimum halo mass that contains a cold, dense gas core; $f_{\rm cd}$ is the fraction of gas that is cold and dense; and $F_{\rm LW}$ is the flux within the LW band in units of 10^{-21} ergs s^{-1} cm^{-2} Hz^{-1}. For our calculation, we consider $f_{\rm cd} = 0.02$, which is a conservative estimate in which we have an adequate source of star-forming gas. With our chosen $f_{\rm cd}$ and no UV background, a $1.74\times10^5\ M_\odot$ halo will form a cold, dense core, which will continue to form a primordial star. In a typical UV background of $J = 10^{-21}$ ergs s^{-1} cm^{-2} Hz^{-1} sr^{-1}, the minimum mass is $4.16\times10^6\ M_\odot$. In addition, minihalos can only form a star within neutral regions of the universe since they are easily photoionized (Haiman et al. 2001; Oh & Haiman 2003), and H I is a necessary ingredient for producing H_2.

Numerical simulations (e.g., Abel et al. 2002; Bromm et al. 2002) illustrated that fragmentation within the inner molecular cloud does not occur and a single massive ($M \sim 100\ M_\odot$) star forms in the central regions. These stars produce hard spectra and tremendous amounts of ionizing photons. For example, the ionizing photon–to–stellar baryon ratio $n_\gamma \sim 91300$, 56700, and 5173 for H, He, and He$^+$ in a 200 $M_\odot$ star (Schaerer 2002). We calculate the ionizing photon flux by considering

$$\left(\frac{dN_\gamma}{dt}\right)_{\rm mini} = \bar{Q} T_{\rm life} \frac{d\rho_{\rm mini}}{dz}\frac{dz}{dt}, \quad (2)$$

where N_γ is the total number of ionizing photons in the universe, $\bar{Q}$ is the time-averaged photon flux, $T_{\rm life}$ is the stellar lifetime, and $\rho_{\rm mini}$ is the comoving number density of minihalos that we determine from an ellipsoidal variant of Press-Schechter (PS) formalism (Press & Schechter 1974; Sheth & Tormen 2002).

The primordial initial mass function (IMF) is unknown; therefore, we assume a fixed primordial stellar mass for each calculation. We run the model for primordial stellar masses $M_{\rm fs}$ of 100, 200, and 500 $M_\odot$ and use the time-averaged emissivities from metal-free stellar models with no mass loss (Schaerer 2002). In our models, the minihalo is quickly ionized and all photons escape into the IGM (Whalen et al. 2004). Furthermore, we use a blackbody spectrum at 10^5 K to approximate the spectrum of the primordial star since surface temperatures are virtually independent of mass at $M \gtrsim 80\ M_\odot$.

2.2. *Star Formation in Protogalaxies*

In $T_{\rm vir} > 10^4$ K halos, baryons can cool efficiently through atomic line cooling, thus fragmenting and forming stars. As described in Haiman & Loeb (1997), we parameterize the properties of these stars by a couple of factors.

2.2.1. *Star Formation Efficiency*

High-redshift galaxies appear to have properties similar to those of local dwarf galaxies. We can constrain the star formation efficiency $f_\star$ by letting local observations guide us. In these galaxies, $f_\star$ ranges from 0.02 to 0.08 (Taylor et al. 1999; Walter et al. 2001). Using the orthodox Schmidt star formation law in local dwarf galaxies, Gnedin (2000) estimated $f_\star$ to be 0.04 if it was constant over the first 3 Gyr, but it can also be as low as 0.022. It should be noted that $f_\star$ can be higher if star formation ceased after a shorter initial burst.

Analyses of metallicities in local dwarf galaxies reveal their prior star formation. Both Type Ia and Type II SNe contribute iron to the IGM, but Type II SNe provide most of the α-process elements (e.g., C, N, O, Mg) to the IGM. Type II SNe occur on timescales $<3\times10^7$ yr, while Type Ia are delayed by 3×10^7 yr to a Hubble time (Matteucci & Recchi 2001). Therefore, we expect an overabundance of α-process elements with respect to iron just after the initial starburst. Plots of [α/Fe] versus [Fe/H][1] help us inspect the evolution of the ISM/IGM metallicity. If the prior star formation is inefficient (i.e., spirals and irregulars), [α/Fe] is only shortly overabundant, which is characterized by a short plateau versus [Fe/H]. On the other hand, if the star formation is fast and occurs early in the lifetime of the galaxy, [α/Fe] remains in the plateau longer due to the quick production of metals by Type II SNe (see Fig. 1 in Matteucci 2003). Also, Venn et al. (2004) discovered no apparent plateau in [α/Fe] versus [Fe/H] comparisons in dwarf spheroidal and irregular galaxies. They conclude that star formation must have been on timescales longer than Type Ia SNe enrichment, which hints at a low and continuous star formation rates in these protogalaxies when compared to recent star formation.

These low star formation efficiencies are further supported by the galaxies contained in the Sloan Digital Sky Survey (SDSS; York et al. 2000). Star formation efficiencies within low-mass galaxies ($M < 3\times10^{10}\ M_\odot$) decline as $M^{2/3}$ (Kauffmann et al. 2003). At high redshift and before reionization, most of the protogalaxies tend to be a few $\times\ 10^7\ M_\odot$, which is comparable to many local dwarf galaxies (Mateo 1998). It should also be noted that no star formation history is alike within individual Local Group galaxies, but it is worthwhile to adopt a global star formation efficiency and observe the consequences on reionization and primordial star formation. With the stated constraints, we set $f_\star = 0.04$ in our main model in concordance with the Schmidt law (Gnedin 2000) and stellar abundances (Venn et al. 2004).

2.2.2. *Stellar Luminosities*

We consider multiple IMFs for star formation within protogalaxies. Our main model uses a Salpeter IMF with a slope $\alpha = -2.35$, metallicity $Z = 10^{-7}, 10^{-5}$, and 0.0004, and $(M_{\rm low},\ M_{\rm up}) = (1,\ 100)\ M_\odot$. We take the continuous starburst spectrum evolution from these particular IMFs that were calculated with Starburst99 (Schaerer 2003; Leitherer et al. 1999). To estimate the ionizing photon per stellar baryon ratio n_γ and luminosities of the IMF at a particular metallicity, we interpolate in $\log_{10}$ space between the two adjacent IMFs. When $Z < 10^{-7}$, we consider the $Z = 10^{-7}$ IMF. The properties of these IMFs are listed in Table 1. Note that more metal-rich starbursts result in a softer spectrum and less ionizing photons in which $n_{\gamma,\rm H}$ decreases almost by a factor of 2.

In the $Z = 0.0004$ IMF, we retain the luminosity from the $Z = 10^{-5}$ one and set $n_{\gamma,\rm He^+} = 0$. We choose to do so because of the theoretical uncertainty of hot Wolf-Rayet (W-R) stars and their presence (for a review, see Schaerer 2000). In Schaerer (2003), the luminosity and spectral hardness increases due to the presence of W-R stars at higher metallicities. However, Smith et al. (2002) calculate W-R spectra that are significantly softer.

2.2.3. *Ionizing Photon Escape Fraction*

Radiation emitted by these stars has a probability $f_{\rm esc}$ of escaping from the protogalaxy and ionizing the IGM. The protogalaxy ISM density and composition plays the biggest role in determining this factor. Heckman et al. (2001) showed that local and distant starburst galaxies, including the gravitationally lensed galaxy MS 1512–cB58 ($z = 2.7$), have $f_{\rm esc} \lesssim 0.06$. This result agrees with previous analyses of $f_{\rm esc}$ in the Lyman continuum (Leitherer et al. 1995; Hurwitz et al. 1997). However, Lyman break galaxies may have $f_{\rm esc} \gtrsim 0.2$ (Steidel et al. 2001). In conjunction with $f_\star = 0.04$ and $M_{\rm fs} = (100,\ 200,\ 500)\ M_\odot$, the choice of $f_{\rm esc} = (0.050,\ 0.033,\ 0.028)$, respectively, in our calculation results in the same optical depth from *WMAP*, $\tau_{\rm es} = 0.17$; thus we use these values in the main models. Wood & Loeb (2000) and Ricotti & Shull (2000) have argued that the escape fraction may be very small due to the much higher densities at high redshift. However, the shallow potential wells and their small size make them susceptible to photoevaporation and effects of radiation pressure (Haehnelt 1995). Other uncertainties such as dust content, metallicity, and whether the ISM density scales as $(1 + z)^3$ blur our intuition about the escape of ionizing radiation. Therefore, we allow $f_{\rm esc}$ to vary from 0.001 to 0.25 since it is unclear whether high-redshift, low-mass protogalaxies allow photons to escape due to self-photoevaporation or absorb the photons due to a higher proper gas density when compared to starburst galaxies.

TABLE 1

Ionizing Photon Production per Stellar Baryon and Luminosities for Metal-poor IMFs

Z	$n_{\gamma,\rm H}$	$n_{\gamma,\rm He}$	$n_{\gamma,\rm He^+}$	$\log \mathcal{L}$ (ergs s^{-1} $M_\odot^{-1}$)
10^{-7}.....	20102	8504	8	36.20
10^{-5}.....	15670	5768	0.2	36.16
0.0004.....	13369	3900	0	36.28[a]

[a] See text for discussion of value.

2.2.4. *Ionizing Photon Rates*

These factors are multiplicative in the amount of radiation that is available from protogalaxies to ionize the IGM. The rate of photons emitted that can ionize species X is

$$\left(\frac{dN_\gamma}{dt}\right)_{\rm proto} = \rho_0 \frac{f_{\rm esc} f_\star n_{\gamma,\rm X}}{\mu m_p} \frac{d\psi_{\rm proto}}{dz}\frac{dz}{dt}, \qquad (3)$$

where μ is the mean molecular weight, $\rho_0 = \Omega_b(3H_0^2/8\pi G)$, m_p is the mass of a proton, and $\psi_{\rm proto}$ is the mass fraction contained in protogalaxies that is calculated by PS formalism. We restrict the product of $f_{\rm esc}$ and $f_\star$ to be in a range from 10^{-4} to 10^{-2} since the resulting reionization histories fall within the measured $\tau_{\rm es}$ error bars. The reionization epoch greatly depends on the factors $f_{\rm esc}$ and $f_\star$. In order to explore the consequences of different values of $\tau_{\rm es}$ and their resulting SNe rates, we vary the factors $f_{\rm esc}$ and $f_\star$.

2.3. *Clumping Factor*

Overdense regions experience an increased recombination rate. Overdensities are characterized by the gas clumping factor $C = \langle n_{\rm H}^2\rangle/\langle n_{\rm H}\rangle^2$, and the recombination rate is increased by this factor. To calculate this parameter in our model, we utilize the same cosmological Eulerian AMR code ENZO (Bryan & Norman 2000) as in Machacek et al. (2001) in a 256^3 simulation with a comoving box side of 500 kpc, eight levels of refinement, and the previously specified cosmological parameters. The top

[1] We use the conventional notation, $[{\rm X/H}] \equiv \log({\rm X/H}) - \log({\rm X_\odot/H_\odot})$.

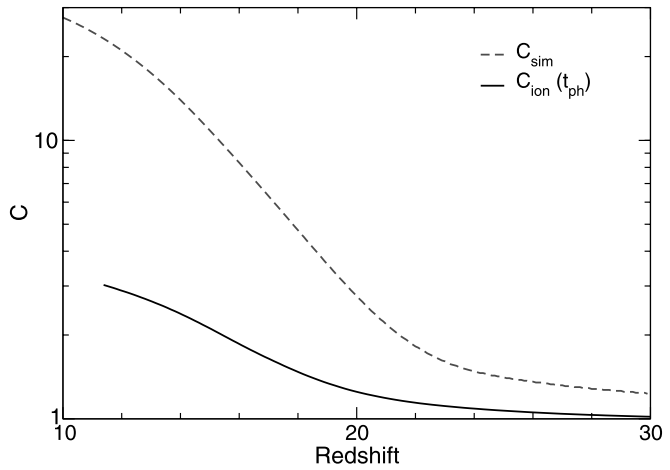

FIG. 1.—*Dashed line*: Gas clumping factor as calculated in our adiabatic hydrodynamic AMR simulation. *Solid line*: Our estimate of the clumping factor in the ionized region, using eq. (5). [*See the electronic edition of the Journal for a color version of this figure.*]

grid has a total (gas) mass resolution of 1013 (135) $M_\odot$, which is smaller than the cosmological Jeans mass

$$M_{\rm J} \approx 10^4 \left(\frac{\Omega_M h^2}{0.15}\right)^{-1/2} \left(\frac{\Omega_b h^2}{0.02}\right)^{-3/5} \left(\frac{1+z}{11}\right)^{3/2} M_\odot. \quad (4)$$

Thus, we account for all collapsed halos in our clumping factor calculation. The simulation is purely adiabatic with no background radiation or atomic/molecular cooling. We show the clumping factor in our simulation, $C_{\rm sim}$, in Figure 1. Cooling only affects localized regions of star formation and does not contribute greatly to the boosting of C. However, ionizing radiation causes photoevaporation of halos, which decreases C in the process (Haiman et al. 2001). We correct for this process by considering that all minihalos with $M_{\rm J} < M < M_{\rm min}$ are photoevaporated in the ionized regions of the universe. For simplicity, we assume that the IGM has a clumping factor of unity, although underdense regions in the IGM correspond to $C_{\rm IGM} \lesssim 1$. We concentrate on the gas clumping factor in the ionizing regions since the goal is to calculate the increase in recombination rates. Consider an ionized region whose volume filling fraction $F_{\rm H}$ is increasing. The evolution of the gas clumping factor is

$$\dot{C} = C_{\rm sim}\dot{F}_{\rm H} - \frac{C-1}{t_{\rm ph}}. \quad (5)$$

The first term accounts for the expansion that will incorporate unaffected, clumpy material into the region, and the second term represents the photoevaporation of overdensities. Any overdensities in the ionized region will be photoevaporated by a background UV flux in approximately a sound-crossing time of the halo,

$$t_{\rm ph} \approx \beta \frac{R_{\rm vir}}{10\ {\rm km\ s^{-1}}}, \quad (6)$$

where β is a normalization factor that accounts for the differences in halo densities at various redshifts and masses, and $R_{\rm vir}$ is the mean virial radius of halo with $M_{\rm J} < M < M_{\rm min}$ (Haiman et al. 2001). Since β remains within ~15% of unity for minihalos, we infer $\beta = 1$.

The effect from photoevaporation is illustrated in Figure 1. Overdensities that are engulfed by ionized regions cannot sufficiently increase the gas clumping factor to overcome the photoevaporation that occurs, and C remains within the range 1–3 for the entire calculation in our main model. This equation is weakly sensitive to $t_{\rm ph}$ since varying $t_{\rm ph}$ by a factor of 6 alters C only by a factor of 2. In a later paper, we shall computationally address the effect of radiation on the clumping factor.

2.4. *The Evolution of UV Background and Halo Densities*

We initialize the following method at $z = 75$ with no UV background, evolve the UV background at the questioned redshift, and repeat the described procedure until cosmological hydrogen reionization occurs.

Given a minimum mass of a star-forming halo, we can exploit PS formalism to calculate number densities of these halos. For minihalos, we calculate their number densities for halos with masses above $M_{\rm min}$ (eq. [1]) and virial temperatures below 10^4 K. Likewise, the protogalaxy mass fraction is calculated by considering all halos more massive than a corresponding $T_{\rm vir} = 10^4$ K.

We choose a variant of PS formalism, which is an ellipsoidal collapse model that is fit to numerical simulations (Sheth & Tormen 1999, 2002; Sheth et al. 2001). This model is concisely summarized in Mo & White (2002). In minihalos, it is reasonable to assume that one star forms per halo since $E_{\rm bind} \lesssim E_{\rm SNe}$, where $E_{\rm bind}$ and $E_{\rm SNe}$ are the binding energy of the host halo and kinetic energy of the primordial SNe, respectively. The gas is totally disrupted in the halo and requires ~100 Myr, which is approximately the Hubble time at cosmological reionization, to recollapse (T. Abel et al. 2002, unpublished). Therefore,

$$\frac{d\rho_\star}{dz} = \frac{d\rho_{\rm mini}}{dt}\frac{dt}{dz}, \quad (7)$$

where $\rho_\star$ is the comoving density of primordial stars.

We evolve the spectrum from early stars to investigate how the UV background behaves, particularly in the LW band, with the cosmological radiative transfer equation

$$\left(\frac{\partial}{\partial t} - \nu H \frac{\partial}{\partial \nu}\right) J = -3HJ - c\kappa J + \frac{c}{4\pi}\epsilon, \quad (8)$$

where $H = H(z) = 100hE(z)$ is the Hubble parameter, and $E(z) = [\Omega_\Lambda + \Omega_m(1+z)^3]^{1/2}$. Here $J = J(\nu, z)$ is specific intensity in units of ergs s^{-1} cm^{-2} Hz^{-1} sr^{-1}, κ is the continuum absorption coefficient per unit length, and $\epsilon = \epsilon(\nu)$ is the proper-volume–averaged emissivity in units of ergs s^{-1} cm^{-3} Hz^{-1} (Peebles 1993). We define the luminosity of the objects as

$$L(\nu) = \begin{cases} 4\pi R^2 B_\nu (T = 10^5\ {\rm K}) & ({\rm mini}), \\ f_{{\rm O}\star} f_\star \mathcal{L} \dfrac{B_\nu (T = 23000\ {\rm K})}{B_\nu (\nu = 2.7kT/h_{\rm P},\ T = 23000\ {\rm K})} & ({\rm proto}), \end{cases}$$

where B_ν is a blackbody spectrum and $\mathcal{L}$ is listed in Table 1. Here R is the radius of the primordial star (Schaerer 2002), $f_{{\rm O}\star}$ is the fraction of O stars in the starburst (Schaerer 2003), and k and $h_{\rm P}$ are Boltzmann's constant and Planck's constant, respectively. For the protogalaxies, $T \sim 23000$ K because the spectrum in the LW band will be dominated by OB stars, and we weight the luminosity by this blackbody spectrum. Emissivity will be nearly zero above 13.6 eV in the neutral universe due to hydrogen and helium absorption.

Photons from primordial stars and protogalaxies between 13.6 eV and several keV ionize the surrounding neutral medium. Using the intrinsic $\geq$13.6 eV ionizing photon rates from primordial stars (eq. [2]) and protogalaxies (eq. [3]), we calculate a

volume-averaged neutral fraction. The change of ionized hydrogen comoving density due to photodissociation and recombination is

$$\frac{dn_{\rm H\,II}}{dt} = -\frac{dN_\gamma}{dt} + Ck_{\rm rec}(1+z)^3 n_{\rm H}^2 \left(1 - \frac{n_{\rm H\,II}}{n_{\rm H}}\right)^2, \quad (9)$$

where $n_{\rm H\,II}$ and $n_{\rm H} = 0.76\rho_0/m_p$ are the ionized and total hydrogen comoving density, dN_γ/dt is the rate of ionizing photons from primordial stars and protogalaxies, C is the clumping factor, and $k_{\rm rec} = 2.6\times10^{-13}$ s^{-1} cm^{-3} is the case B recombination rate of hydrogen at $T \approx 10^4$.

In the case for once-ionized helium, $k_{\rm rec}$ is approximately equal to the hydrogen case, but since the helium number density is less than hydrogen, less recombinations occur. Naively, this will result in a higher He^+ fraction than H^+ due to the hardness of the primordial radiation. Realistically, when the ionizing photons reach the ionization front they will ionize either helium or hydrogen since hydrogen still has a finite photoionization cross section above 23.6 eV. We consider the He^+ regions to be equal to the H^+ regions. Then we add $N_{\gamma,\rm He}$ to $N_{\gamma,\rm H}$ to compensate for this effect. We perform a similar analysis on doubly ionized helium in which $k_{\rm rec,He^+} = 1.5\times10^{-12}$ s^{-1} cm^{-3}, but we evaluate equation (9) directly with $N_{\gamma,\rm He^+}$.

The absorption coefficient in equation (8) is ignored since we take into account the Lyman series line absorption by the following procedure. Photons with 11.26 eV $< E <$ 13.6 eV escape into the IGM, which will photodissociate H_2. To calculate the flux within the LW band, we must consider the processing of photons by the Lyman series transitions (Haiman et al. 1997). Before reionization, these transitions absorb all photons at their respective energies. These absorbers can be visualized as optically thick "screens" in redshift space, for which the photon must have been emitted after the farther wall in redshift. This process creates a "sawtooth" spectrum with minimums at redshift screens, which is illustrated in Figure 2. For instance, an observer at $z = 20$ observes photons at 12.5 eV; it must have been emitted by the Lyγ line at 12.75 eV at $z = 20.4$. The fraction of photons that escape from these walls during an integration step is

$$f = \frac{1 - [(1+z)/(1+z_{\rm screen})]^{1.5+\alpha}}{1 - [(1+z)/(1+z+\Delta z)]^{1.5+\alpha}}, \quad (10)$$

where $\alpha = -1.8$ is the slope of a power-law spectrum ($F_\nu \propto \nu^{-\alpha}$) and

$$z_{\rm screen} = \frac{\nu}{\nu_{{\rm Ly}i}}(1+z_{\rm obs}) - 1; \quad (11)$$

$\nu_{{\rm Ly}i}$ is the nearest, blueward Lyman transition to ν. Inherently, $z_{\rm screen}$ must be between z and $z + \Delta z$.

Considering the processes described above, we finally evolve the UV background with the volume-averaged emissivity,

$$\epsilon_{\rm mini}(\nu) = \rho_{\rm mini}\, L(\nu)\left(1 - \frac{n_{\rm H\,II}}{n_{\rm H}}\right), \quad (12)$$

$$\epsilon_{\rm proto}(\nu) = \nu^{-1}\rho_0 \frac{d\psi_{\rm proto}}{dt} L(\nu, f_\star), \quad (13)$$

$$\epsilon(\nu) = (1+z)^3\left[\epsilon_{\rm mini}(\nu) + \epsilon_{\rm proto}(\nu)\right] f(\nu). \quad (14)$$

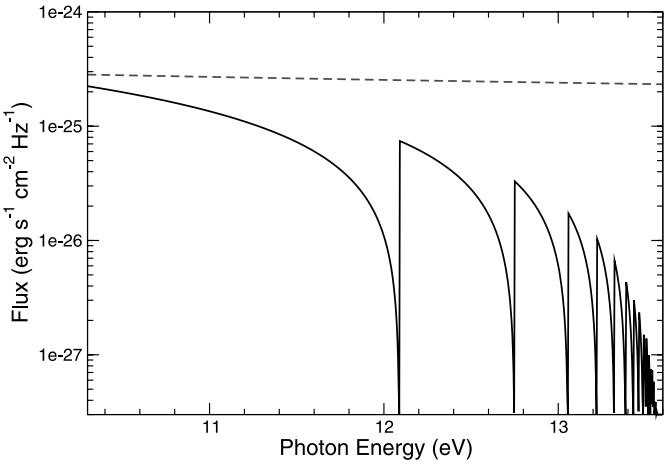

FIG. 2.—*Dashed line*: Example unprocessed spectrum of a continuous source of radiation. After being absorbed and reemitted by Lyman series transitions, it transforms into the sawtooth spectrum (*solid line*). This particular spectrum is for $z_{\rm on} = 30$ and $z_{\rm obs} = 20$. [*See the electronic edition of the Journal for a color version of this figure.*]

3. RESULTS

In this section, we present the results of our calculation of the evolution of SN rates and the UV background. We also present the variance of optical depth to electron scattering and SN rates with different primordial and protogalaxy star formation scenarios. In Figure 3 we plot minimum halo masses that host primordial stars, densities of those halos, SN rates, and the UV background in the LW band for the main models.

3.1. *Optical Depth to Electron Scattering*

Optical depth due to electron scattering,

$$\tau_{\rm es}(z) = \int_0^z \bar{n}_e \sigma_{\rm Th} c \left(\frac{dt}{dz}\right) dz, \quad (15)$$

where n_e and $\sigma_{\rm Th}$ are the proper electron density and Thomson cross section, respectively, is a good observational test to determine the neutral fraction of the universe before reionization. The *WMAP* satellite measured $\tau_{\rm es}(z) = 0.17 \pm 0.04$ at 68% confidence.

To accurately calculate n_e, we must consider all ionizations of primordial gas, which includes H^+, He^+, and He^{++}. Therefore, the proper electron density is

$$n_e = (1+z)^3(n_{\rm H}F_{\rm H^+} + n_{\rm He}F_{\rm He^+} + 2n_{\rm He}F_{\rm He^{++}}), \quad (16)$$

where $F_{\rm H^+}$, $F_{\rm He^+}$, and $F_{\rm He^{++}}$ are the ionized volume fraction of H^+, He^+, and He^{++}, respectively. The effect of more luminous primordial stars is evident in Figure 4 as they ionize the universe faster at high redshifts. To match the *WMAP* result, fewer ionizing photons are required from protogalaxies if the primordial IMF is skewed toward higher masses. Although these models have the same total $\tau_{\rm es}$, cosmological reionization occurs at $z =$ 13.7, 11.6, and 11.2 for $M_{\rm fs} = 100$, 200, and 500 $M_\odot$, respectively. However, these reionization redshifts are not consistent with observed Gunn-Peterson troughs in $z \sim 6$ quasars (Becker et al. 2001; Fan et al. 2002) and the high IGM temperatures at $z \sim 4$ inferred from Lyα clouds (Hui & Haiman 2003). Perhaps portions of the universe recombine after complete reionization, which will match the most distant quasar observations (Cen 2003b). If this were true, the first reionization epoch has to be

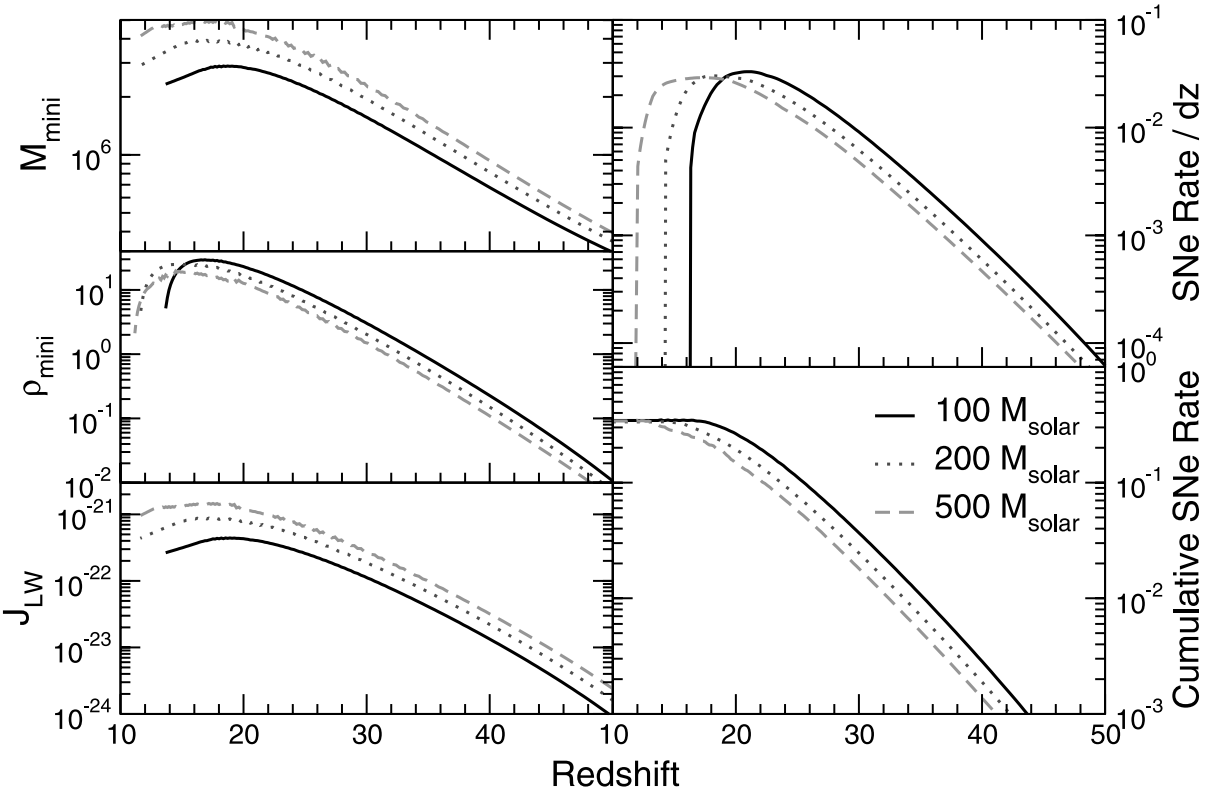

FIG. 3.—*Clockwise from upper right*: Primordial SN rates (yr^{-1} deg^{-2}) per unit redshift, cumulative primordial SN rate (yr^{-1} deg^{-2}), specific intensity (ergs s^{-1} cm^{-2} Hz^{-1} sr^{-1}) in the LW band, comoving density (Mpc^{-3}) of halos above the critical star formation mass in neutral regions, and critical halo mass ($M_\odot$) for primordial star formation. The solid, dotted, and dashed lines correspond to calculations run with a fixed primordial stellar mass of 100, 200, and 500 $M_\odot$, respectively. [*See the electronic edition of the Journal for a color version of this figure.*]

faster and earlier to compensate for this partial recombination and to match the *WMAP* result. This would lower our SNe rates slightly since primordial star formation will be further suppressed by the quicker reionization.

The ionizing history of the universe is directly related to the number of ionizing photons that are produced and escape into the IGM. If we fix $\tau_{es} = 0.17$, we constrain $f_\star$ and f_{esc} to a power law

$$f_{esc} = B f_\star^{-a}, \tag{17}$$

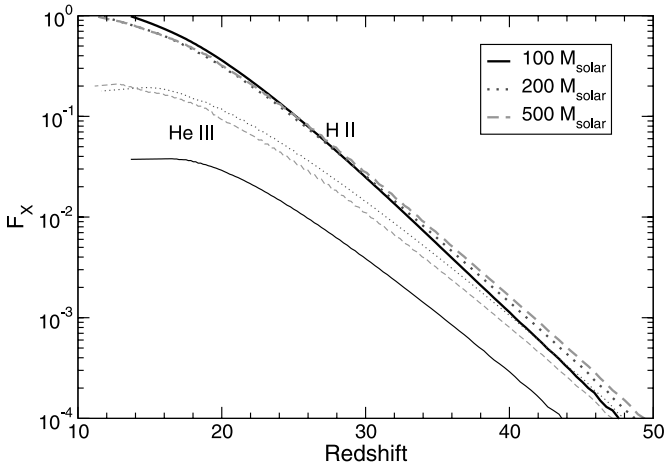

FIG. 4.—Evolution of filling factors of ionized hydrogen (*upper lines*) and doubly ionized helium (*lower lines*). The meaning of the lines is the same as in Fig. 3. [*See the electronic edition of the Journal for a color version of this figure.*]

where $B = (0.00307,\ 0.00239,\ 0.00217)$ and $a = (0.906,\ 0.839,\ 0.806)$ for primordial stellar masses 100, 200, and 500 $M_\odot$, respectively. The flattening of the power law with increasing M_{fs} indicates the increasing ionizing contribution from primordial stars.

3.2. *Primordial Supernova Rates*

The natural units in our computation is comoving density, yet a more useful unit is observed SNe yr^{-1} deg^{-2}. First we assume that these SNe are bright for 1 yr and then correct for time dilation. We consider the equation

$$\frac{d^2N}{dt\,dz} = \frac{dV_c}{dz}\frac{d\rho_\star}{dt}(1+z)^{-1}, \tag{18}$$

where $(1+z)^{-1}$ converts the proper SN rate into the observer time frame, and

$$\frac{dV_c}{dz} = D_H \frac{(1+z)^2 D_A^2}{E(z)}\Omega \tag{19}$$

is the comoving volume element. Here Ω ($deg^2 = 3.046\times10^{-4}$ sr) is the solid angle of sky that we want to sample, $D_H = c/H_0$ is the Hubble distance, $D_A = D_M/(1+z)$ is the angular diameter distance, and $D_M = D_H \int_0^z E^{-1}(z')dz'$ is the comoving distance (Peebles 1993). The above equations are only valid for a flat ΛCDM universe.

Since we only allow primordial stars to form in neutral regions, SN rates from these stars are highly dependent on f_{esc} and $f_\star$ but less sensitive to the stellar primordial mass M_{fs}. In our main models, the SN rate varies little with primordial stellar

TABLE 2

GAUSSIAN FITS TO $M_{\rm min}$ FOR THE MAIN MODELS, $\log(M) = A\exp[-(z-z_0)^2/(2\sigma^2)] + C$

$M_\odot$	A	z_0	σ	C
100.....	1.67 ± 0.01	10.0 ± 0.2	21.9 ± 0.1	5.19 ± 0.01
250.....	1.71 ± 0.00	10.5 ± 0.0	23.3 ± 0.0	5.16 ± 0.00
500.....	1.72 ± 0.01	11.3 ± 0.2	23.5 ± 0.1	5.15 ± 0.00

mass and is 0.34 $\rm yr^{-1}\ deg^{-2}$. Even if we vary $f_\star$ in a range 0.01–0.1 and fix $\tau_{\rm es}$, primordial SN rates do not vary more than 10% from the main models when constrained by *WMAP*. As $f_{\rm esc}$ increases, the SN rates decrease due to a higher ionized volume filling factor. The effect of a higher $f_\star$ squelches SN rates by two processes, a higher ionized filling factor and higher UV background, which restricts primordial stars to forming in more massive halos.

The primordial SN rate peaks at $z \sim 14$–20, earlier epochs for larger primordial stellar masses, and falls sharply afterward due to the ensuing cosmological reionization. Primordial star formation ceases after $z \sim 12$–16. The combination of an increasing UV background, reionizing universe, and disruption of minihalos from primordial SNe suppresses all primordial star formation. For each main model, we fit a Gaussian curve to the minimum mass of a minihalo that can host a primordial star, and the parameters are listed in Table 2 and are valid for $z > z_0$.

It is fascinating that some rare primordial SNe occur at $z \gtrsim 40$. As an exercise, we estimate the earliest epoch of minihalo star formation in the visible universe with PS formalism and by considering that it takes ∼9.33 Myr for a halo to form a protostellar core (Abel et al. 2002). With PS formalism, the "first" epoch equals where the minihalo density is the inverse of the comoving volume inside $z = 1000$ (10,523 $\rm Gpc^3$). Then we include an additional 9.33 Myr for the ensuing star formation. The halo masses of 1.74×10^5 and $10^6\ M_\odot$ correspond to formation times of $z \sim 71$ and 64, respectively. Another interesting event to calculate is when the SN rate equals one per sky per year, which occurs at $z \sim 51$ when considering the collapse and star formation timescales. This epoch is in agreement with the Miralda-Escudé (2003) estimate of $z \simeq 48$.

Furthermore, using the proper minihalo density we calculate the average light-travel time between sources, which indicates when negative H_2 feedback first affects star formation. Star formation occurs ∼9.33 Myr after halo formation, so radiation escapes into the IGM at a time $t_{\rm rad} = t_H(z_{\rm form}) + 9.33$ Myr, where $z_{\rm form}$ is the halo formation redshift. These sources have a mean proper separation of $d = \rho_\star^{-1/3}/(1+z)$; therefore the time when radiation influences other halos is $t_{\rm rad} + d/c$. The minimum of this time, corresponding to $z = 54$, is when radiation reaches other halos for the first time. We illustrate the mean proper separation and epoch of first-radiation effects in Figure 5.

3.3. *Magnitudes and Observability*

The magnitudes of primordial SNe are as important as their occurrence rates to catch these events unfolding in the distant universe. We exploit the ^{56}Ni output from metal-free SN models to calculate luminosities $L(t)$ from the two-step decay of ^{56}Ni to ^{56}Fe (Heger & Woosley 2002). We consider the emission spectrum to be a blackbody spectrum with a time-dependent temperature

$$T(t) = \left[\frac{L(t)M}{8\pi\sigma E t^2}\right]^{1/4}(1+z), \qquad (20)$$

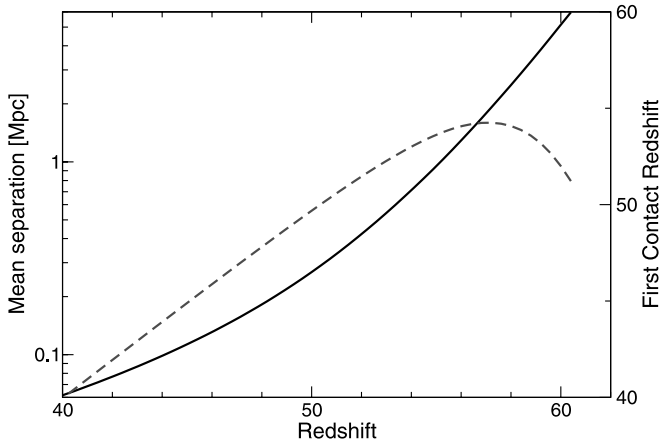

FIG. 5.—*Solid line*: Mean proper separation between minihalos. *Dashed line*: Redshift at which minihalos first receive radiation from neighboring sources forming at the same epoch. [*See the electronic edition of the Journal for a color version of this figure.*]

where M and E are the stellar mass and kinetic energy of the SNe, respectively, calculated using free expansion arguments. The temperature and luminosity of a 175, 200, and 250 $M_\odot$ primordial-star SN are depicted in Figure 6. For comparison, we plot the typical light curve for a Type Ia SN. Kinetic energy is taken from the SN models (Heger & Woosley 2002). We consider the SN remnant to be in free expansion for the first year because radiation from the primordial star should expel most of surrounding medium to create a low-density, highly ionized region of approximately 100 pc in size for a 120 $M_\odot$ primordial star (Whalen et al. 2004).

In the upper range ($M > 200\ M_\odot$) of pair-instability SNe, these events produce 1–57 $M_\odot$ of ^{56}Ni (Heger & Woosley 2002), which will produce tremendous luminosities when compared to typical Type II SN outputs of only 0.1–0.4 $M_\odot$ (Woosley & Weaver 1986). However, uncertainty in the primordial IMF places doubt on the frequency of primordial-star SNe with high ^{56}Ni yields. Using conventional Type II SN parameters of $L \simeq 3\times10^{42}$ ergs $\rm s^{-1}$, $T = 25000$ K (2 days $\lesssim t \lesssim$ 7 days), and

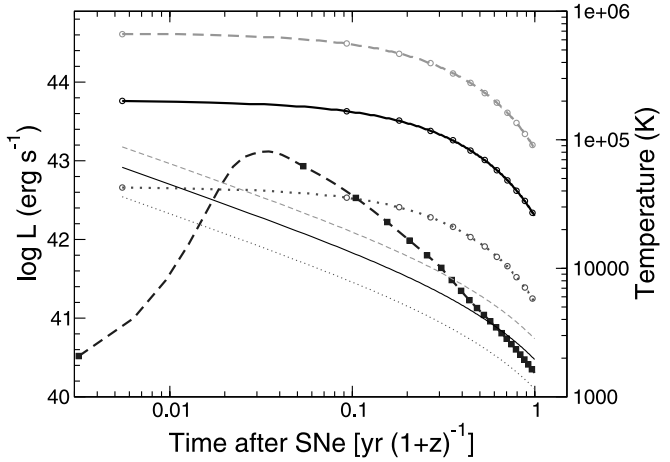

FIG. 6.—Using the decay of ^{56}Ni and eq. (20), we calculate the luminosity of primordial SNe and its effective temperature. Heavy, upper lines with circles show luminosities, and light, lower lines show temperatures. The black dashed line with filled squares shows a Type Ia luminosity evolution for comparison (Woosley & Weaver 1986). The lines from top to bottom (dashed, solid, and dotted) are for stellar masses of 175, 200, and 250 $M_\odot$. [*See the electronic edition of the Journal for a color version of this figure.*]

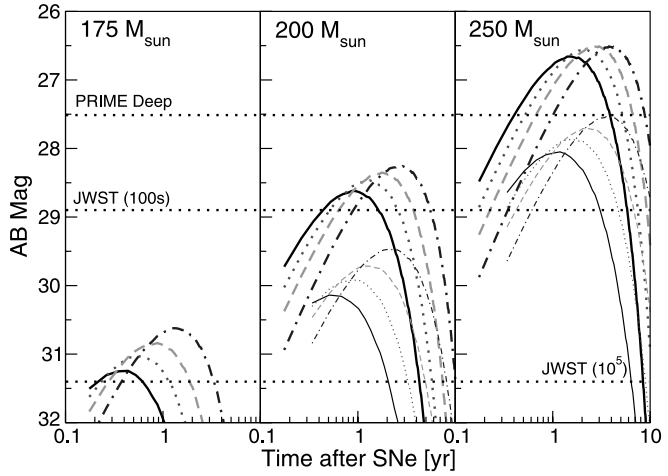

FIG. 7.—*Left to right*: Magnitudes for $M_{\rm fs} = 175$, 200, and 250 $M_\odot$. The dotted horizontal lines indicate limiting magnitudes of space infrared observatories. The heavy, upper lines and light, lower lines show SNe at $z = 15$ and 30, respectively. The magnitude for the 175 $M_\odot$ and $z = 15$ case is not shown since it is too dim. The solid, dotted, dashed, and dash-dotted lines are for *Spitzer* wave bands centered at 3.56, 4.51, 5.69, and 7.96 μm, respectively. Note that the detection limits of *Spitzer* and the *PRIME* medium survey are not shown since they are too high at 24.5 and 25.6, respectively. [*See the electronic edition of the Journal for a color version of this figure.*]

$T = 7000$ K (7 days $\lesssim t \lesssim$ 2 months) that are tuned by observed light curves, Miralda-Escudé & Rees (1997) determine apparent magnitudes that are 1–3 mag lower than our values, which are brighter due to the greater nickel production of pair-instability SN models. Their model should apply to the pair-instability SNe with little ^{56}Ni ejecta. Furthermore, our temperatures are higher due to the greater amount of ^{56}Ni decay in pair-instability SNe.

In typical Type II light curves, radioactive decay does not significantly contribute to the luminosity in the plateau stage (Popov 1993). In primordial SNe, the ^{56}Ni decay may overwhelm the typical sources of energy within the expanding fireball and create a totally different light curve. We stress that our light curve is a very rough estimate of the processes occurring within a primordial SN.

In Figure 7 we compare maximum AB magnitudes of low- and high-mass pair-instability SNe at various redshifts and sensitivities of space infrared observatories. We consider the sensitivities of *Spitzer* at 3.5 μm, *PRIME* medium and deep surveys, and *JWST* with exposure times of 100 and 10^5 s. Our simple estimate leads to very high predicted luminosities, and more detailed numerical models of these explosions are clearly desirable.

4. DISCUSSION

Other factors could alter the feasibility of observing primordial SNe. For instance, $\sim$2% of primordial stars might die in collapsar gamma-ray bursts (GRBs; Heger et al. 2003). Lamb (1999) also provides a ratio of GRBs to Type Ib/c SN rates that is $\sim 3 \times 10^{-5} (\theta_b/10^{-2})^{-1}$, where θ_b is the beaming angle. However, this estimate is for a normal Salpeter IMF, and as mentioned before, the primordial star IMF could be skewed toward high masses, which would increase the probability of a GRB. Zero- and low-metallicity massive stars outside the pair-instability mass range die as GRBs or jet-driven SNe, which are similar to GRBs but not as energetic and spectrally hard. If we consider a proportionality constant $f_{\rm GRB}$ and beaming angle, we estimate that the all-sky primordial GRB rate

$$R_{\rm GRB} = 2.8 \left(\frac{\theta_b}{0.01}\right) \left(\frac{f_{\rm GRB}}{0.02}\right) \ {\rm GRBs\ yr^{-1}}. \qquad (21)$$

In $M \lesssim 140\ M_\odot$ stars, a collapsar results when it forms a proto–neutron star, cannot launch a supernova shock, and directly collapses to form a black hole in $\sim$1 s (Woosley 1993; MacFadyen & Woosley 1999). In $M \gtrsim 260\ M_\odot$ stars, it does not create a proto–neutron star and directly collapses into a massive black hole (Fryer et al. 2001). Afterward, these black holes can accrete gas and produce X-rays that can further ionize the universe (Ricotti & Ostriker 2004b). A few of these X-ray sources could be detected in the Chandra Deep Field (Ricotti et al. 2005; Alexander et al. 2003). In most GRB models (for an overview, see Mészáros 2002), the radiation is beamed to small opening angles due to relativistic effects, which would render a fraction of GRBs to be unobservable in our perspective. Finally, gravitational lensing will significantly increase the apparent magnitudes for selected primordial SNe for very small survey areas. However, the overall magnitude distribution is slightly dimmed by gravitational lensing (Marri & Ferrara 1998; Marri et al. 2000).

Deviations in the amplitudes of fluctuations, σ_8, and a running spectral model (Liddle & Lyth 1992, 1993) also affect primordial SN rates. We ran a set of models with $\sigma_8 = 0.8$, and predictably, the rates decreased by a factor of $\sim$2.5 due to lesser powers at small mass scales. When we match $\tau = 0.17$, rates range from 0.12 to 0.2 yr^{-1} deg^{-2}, with the rates peaking earlier at $z \sim 20$, but now the redshift peaks are nearly independent of redshift with only $\delta z \approx 1$ separating the 100 and 500 $M_\odot$ models. If we keep the protogalaxy parameters from the main models, rates do not change; however, the rates peak later than our main models by $\delta z \approx 4$, and τ lowers to 0.14. According to inflationary models, the spectral index of fluctuations should be slowly varying with scale. While analyzing *WMAP* data, Peiris et al. (2003) determined that the fluctuation amplitude is significantly lower at small scales. With lesser powers at small scales, primordial SN rates decrease as in the case of a lower σ_8. In principle, studying primordial SNe occurrences with respect to redshift could furnish direct constraints on the power spectrum at these small scales.

We have demonstrated our model's dependence on the free parameters $f_{\rm esc}$, $f_\star$, and $M_{\rm fs}$. We now suggest several observational and numerical methods in order to constrain our models. To constrain early star formation history of dwarf irregulars with the [α/Fe] versus [Fe/H] comparison, metal analyses of stars with [Fe/H] < -1.5 are needed to determine early star formation rates of particular systems (see Fig. 1.5 in Venn et al. 2004). Dwarf spheroidals exhibit greater variance in star formation histories from system to system, but a similar study will increase our knowledge of high redshift star formation in these small galaxies to further constrain $f_\star$ at high redshifts. To improve on these studies, the advances in multiobject spectrographs (e.g., VIMOS, FLAMES, and GMOS)[2] enable the gathering of many stellar spectra in one exposure. This will greatly increase the stellar population data of dwarf galaxies.

Since some massive stars die as a long-duration GRB, these events can convey information from the death of Population III

[2] See http://www.eso.org/instruments/vimos, http://www.eso.org/instruments/flames, and http://www.gemini.edu/sciops/instruments/gmos/gmosIndex.html, respectively.

stars. The propagation of the initial burst and afterglow provide information about the total energy, gas density in the vicinity, and Lorentz factor of the beam. The host-galaxy ISM properties will help constrain the $f_{\rm esc}$ in high-redshift galaxies. As in the case of GRB 030329 (Stanek et al. 2003), the power-law spectra of the afterglow can be subtracted to obtain a residual that resembles a typical SN spectrum, which may be used to roughly determine the mass of the progenitor. Observing the afterglow is necessary to determine its redshift. The prospect of observing prompt afterglows will be accomplished easier with *Swift*,[3] which can possibly detect GRB afterglows to $z = 16$ and 33 in the K and M bands, respectively (Gou et al. 2004). Furthermore, $\gtrsim$50% of GRBs occur earlier than $z = 5$, and 15% of those high-redshift GRBs are detectable by *Swift* (Bromm & Loeb 2002). The comparison to nearby SNe can provide crucial information about the high-redshift ISM. Finally, there is the possibility of exploring the intervening absorption with the fast-pointing and multiwavelength observations of *Swift* (Vreeswijk et al. 2003; Loeb 2005; Barkana & Loeb 2004). This IGM absorption would constrain the reionization history of the universe better, which may change the primordial SN rates, but more specifically the rate per unit redshift, which would roughly conform to the filling factor evolution.

The radiation from protogalaxies and primordial stars will not only ionize the universe but also contribute to the near-infrared background (NIRB). Calculations have shown that primordial stars can provide a significant fraction of radiation to the NIRB (Santos et al. 2002; Salvaterra & Ferrara 2003); however, the paradigm of early reionization set by *WMAP* was not considered at the time. The $f_\star$ values of protogalaxies and the densities of primordial stars can be further constrained if future studies of the NIRB consider the large emissivities of zero- and low-metallicity sources at $z \gtrsim 15$.

Other outlooks include detecting high-redshift radio sources and searching for 21 cm absorption and emission (Hogan & Rees 1979; Scott & Rees 1990; Iliev et al. 2003; Furlanetto et al. 2004). By looking for 21 cm signatures, observations would be directly probing the neutral regions of the universe since the Gunn-Peterson trough saturates only at a neutral filling factor of $\sim 10^{-5}$. Finally, additional searches for high-redshift starbursts (e.g., Ellis et al. 2001; Pelló et al. 2004) in lensed fields will furnish an understanding of the characteristics of these objects and help tighten our models of early "normal" and primordial star formation.

Metal-free stars with masses between $\sim$140 and 260 $M_\odot$ result in an SN that is visible and eject heavy elements into the IGM. When a star is within this range, the stellar core has sufficient entropy after helium burning to create positron/electron pairs. These pairs convert the gas energy into mass while not greatly contributing to pressure. This creates a major instability in which the star contracts rapidly until oxygen and silicon implosive burning occurs. Then the star totally disrupts itself by these nuclear explosions and leaves no remnant (Barkat et al. 1967; Bond et al. 1984). Stars between $\sim$100 and 140 $M_\odot$ experience this instability. It is not violent enough to disrupt the star, but pulsations and mass loss occur until equilibrium is reached and the hydrogen envelope is ejected (Bond et al. 1984; Heger & Woosley 2002).

Metal production from primordial stars cannot account for the volume filling factor of metals as seen in Lyα clouds in current models (Norman et al. 2004). To further test our model, we determine a volume-averaged metallicity of $[{\rm Fe/H}] \lesssim -4.1$ using our SN densities and the metal production of pair-instability SNe (Heger & Woosley 2002). Therefore, ubiquitous star formation in protogalaxies most likely polluted the sparse regions of the universe. Combining the primordial and protogalaxy metal output, simulations with proper metal transport should agree with the abundances observed in Lyα clouds. Such simulations that take into account both of these metal sources and match the results of Songaila & Cowie (1996) and Songaila (2001) are needed to constrain star formation before reionization.

Numerical simulations are also needed to investigate radiative transfer from a protogalaxy stellar population. This scenario will contain more complexities than a single primordial star in a spherical halo as in Whalen et al. (2004). With a protogalactic simulation with the Jeans length resolved, star formation and feedback, and radiative transfer, it will be possible to study the evolution of the ISM in a protogalaxy, which will produce insight and better constraints on the photon escape fraction $f_{\rm esc}$ in the Lyman continuum at high redshifts. Ricotti et al. (2002a, 2002b) thoroughly study radiative transfer around protogalaxies; however, in their work $f_{\rm esc}$ is still a parameter, when in fact it should be determined from the radiative transfer results in the simulations. Ideally, the analytical ideas about ionizing the universe in Madau (1995), Haardt & Madau (1996), and Madau et al. (1999) should be realized in such simulations, but in the context of the current paradigm of a high-redshift reionization as indicated by *WMAP*. Also, we may hope by using numerical radiative transfer techniques for line and continuum radiation in three dimensions to push the simulations of Abel et al. (2002) to follow the entire accretion phase of the first stars. This would lead to stronger constraints on the masses of the very first stars.

5. SUMMARY

The *WMAP* measurement of optical depth to electron scattering places a constraint on early cosmological reionization of the universe, which we show to be mainly from star formation in protogalaxies. This general result is in agreement with other studies of reionization after *WMAP* (e.g., Cen 2003a; Somerville & Livio 2003; Ciardi et al. 2003; Ricotti & Ostriker 2004a; Sokasian et al. 2004).

1. The radiation from protogalaxies squelches primordial star formation, and *$\sim$0.34 primordial SNe deg^{-2} yr^{-1}* are expected. SN rates can vary from 0.1 to >1.5 deg^{-2} yr^{-1} depending on the choice of primordial stellar mass and protogalaxy parameters while still constrained by the *WMAP* result. The peak of the SN rate occurs *earlier* with *increasing primordial stellar masses*. These results are upper limits since the rate of visible primordial SNe depends on the IMF because only a fraction will lie in the pair-instability SN mass range. The other massive primordial stars might result in jet-driven SNe or long-duration GRBs.

2. Stellar metal abundances and star formation in local dwarf galaxies aid in estimating protogalaxy characteristics. We choose $f_\star = 0.04$ and $f_{\rm esc} = 0.050$ in our 100 $M_\odot$ model. In protogalaxies, the star formation efficiency is slightly lower than local values, but the photon escape fraction is within local observed fractions.

3. Primordial stars enrich the IGM to a maximum volume-averaged [Fe/H] of about -4.1 if the IMF is skewed toward the pair-instability upper mass range. A proper IMF will lessen this volume-averaged metallicity since only a fraction of stars will exist in this mass range.

4. The entire error bar of the *WMAP* measurement of optical depth to electrons can be explained by a higher/lower $f_\star$

[3] See http://swift.gsfc.nasa.gov.

and f_{esc}. Protogalaxies can ionize the IGM easily since low-metallicity starburst models produce 20%–80% more ionizing photons as previously used ($Z = 0.001$) IMFs. Massive primordial stars provide $\sim$10% of the necessary photons to achieve reionization. No exotic processes or objects are necessary.

5. Only the upper mass range of pair-instability SNe will be observable with *JWST* since the low-mass counterparts do not produce enough ^{56}Ni to be very luminous.

Although the IMF of primordial stars is unknown, simulations have hinted that a fraction of metal-free stars may exist in the pair-instability mass range. When observational rates, light curves, and spectra are obtained from future surveys, these data will provide very stringent constraints on the underlying CDM theory, as well as on our understanding of primordial star formation.

This work was supported by NSF CAREER award AST 02-39709 from the National Science Foundation. J. H. W. also acknowledges support from the Pennsylvania Space Grant Consortium. We thank the anonymous referee for many valuable comments. We are grateful to Alexander Heger for useful discussions about primordial SN luminosities. We are also grateful to Leonidas A. Moustakas for encouraging us to investigate the feasibility of a future detection.

REFERENCES

Abel, T., Anninos, P., Norman, M. L., & Zhang, Y. 1998, ApJ, 508, 518
Abel, T., Bryan, G. L., & Norman, M. L. 2000, ApJ, 540, 39
———. 2002, Science, 295, 93
Alexander, D. M., et al. 2003, AJ, 126, 539
Bardeen, J. M., Bond, J. R., Kaiser, N., & Szalay, A. S. 1986, ApJ, 304, 15
Barkana, R., & Loeb, A. 2004, ApJ, 601, 64
Barkat, Z., Rakavy, G., & Sack, N. 1967, Phys. Rev. Lett., 18, 379
Becker, R. H., et al. 2001, AJ, 122, 2850
Bond, J. R., Arnett, W. D., & Carr, B. J. 1984, ApJ, 280, 825
Bromm, V., Coppi, P. S., & Larson, R. B. 2002, ApJ, 564, 23
Bromm, V., & Loeb, A. 2002, ApJ, 575, 111
Bryan, G. L., & Norman, M. L. 2000, in Structured Adaptive Mesh Refinement (SAMR) Grid Methods, ed. S. B. Baden (New York: Springer), 165
Cen, R. 2003a, ApJ, 591, L5
———. 2003b, ApJ, 591, 12
Ciardi, B., Ferrara, A., & White, S. D. M. 2003, MNRAS, 344, L7
Couchman, H. M. P., & Rees, M. J. 1986, MNRAS, 221, 53
Dekel, A., & Rees, M. J. 1987, Nature, 326, 455
Ellis, R., Santos, M. R., Kneib, J., & Kuijken, K. 2001, ApJ, 560, L119
Fan, X., Narayanan, V. K., Strauss, M. A., White, R. L., Becker, R. H., Pentericci, L., & Rix, H. 2002, AJ, 123, 1247
Field, G. B., Somerville, W. B., & Dressler, K. 1966, ARA&A, 4, 207
Fryer, C. L., Woosley, S. E., & Heger, A. 2001, ApJ, 550, 372
Fuller, T. M., & Couchman, H. M. P. 2000, ApJ, 544, 6
Furlanetto, S. R., Sokasian, A., & Hernquist, L. 2004, MNRAS, 347, 187
Gnedin, N. Y. 2000, ApJ, 535, L75
Gou, L. J., Mészáros, P., Abel, T., & Zhang, B. 2004, ApJ, 604, 508
Haardt, F., & Madau, P. 1996, ApJ, 461, 20
Haehnelt, M. G. 1995, MNRAS, 273, 249
Haiman, Z., Abel, T., & Madau, P. 2001, ApJ, 551, 599
Haiman, Z., Abel, T., & Rees, M. J. 2000, ApJ, 534, 11
Haiman, Z., & Loeb, A. 1997, ApJ, 483, 21
Haiman, Z., Rees, M. J., & Loeb, A. 1997, ApJ, 476, 458
Heckman, T. M., Sembach, K. R., Meurer, G. R., Leitherer, C., Calzetti, D., & Martin, C. L. 2001, ApJ, 558, 56
Heger, A., Fryer, C. L., Woosley, S. E., Langer, N., & Hartmann, D. H. 2003, ApJ, 591, 288
Heger, A., & Woosley, S. E. 2002, ApJ, 567, 532
Hogan, C. J., & Rees, M. J. 1979, MNRAS, 188, 791
Hui, L., & Haiman, Z. 2003, ApJ, 596, 9
Hurwitz, M., Jelinsky, P., & Dixon, W. V. D. 1997, ApJ, 481, L31
Iliev, I. T., Scannapieco, E., Martel, H., & Shapiro, P. R. 2003, MNRAS, 341, 81
Kauffmann, G., et al. 2003, MNRAS, 341, 33
Kogut, A., et al. 2003, ApJS, 148, 161
Lamb, D. Q. 1999, A&AS, 138, 607
Leitherer, C., Ferguson, H. C., Heckman, T. M., & Lowenthal, J. D. 1995, ApJ, 454, L19
Leitherer, C., et al. 1999, ApJS, 123, 3
Liddle, A. R., & Lyth, D. H. 1992, Phys. Lett. B, 291, 391
———. 1993, Phys. Rep., 231, 1
Loeb, A. 2005, in IAU Colloq. 192, Cosmic Explosions: On the 10th Anniversary of SN 1993J, ed. J. M. Marcaide & K. W. Weiler (Berlin: Springer), in press (astro-ph/0307231)
MacFadyen, A. I., & Woosley, S. E. 1999, ApJ, 524, 262
Machacek, M. E., Bryan, G. L., & Abel, T. 2001, ApJ, 548, 509
Madau, P. 1995, ApJ, 441, 18
Madau, P., Haardt, F., & Rees, M. J. 1999, ApJ, 514, 648
Marri, S., & Ferrara, A. 1998, ApJ, 509, 43
Marri, S., Ferrara, A., & Pozzetti, L. 2000, MNRAS, 317, 265
Mateo, M. L. 1998, ARA&A, 36, 435
Matteucci, F. 2003, Ap&SS, 284, 539
Matteucci, F., & Recchi, S. 2001, ApJ, 558, 351
Mészáros, P. 2002, ARA&A, 40, 137
Miralda-Escudé, J. 2003, Science, 300, 1904
Miralda-Escudé, J., & Rees, M. J. 1997, ApJ, 478, L57
Mo, H. J., & White, S. D. M. 2002, MNRAS, 336, 112
Norman, M. L., O'Shea, B. W., & Paschos, P. 2004, ApJ, 601, L115
Oh, S. P., & Haiman, Z. 2003, MNRAS, 346, 456
Peebles, P. J. E. 1993, Principles of Physical Cosmology (Princeton: Princeton Univ. Press)
Peiris, H. V., et al. 2003, ApJS, 148, 213
Pelló, R., Schaerer, D., Richard, J., Le Borgne, J.-F., & Kneib, J.-P. 2004, A&A, 416, L35
Popov, D. V. 1993, ApJ, 414, 712
Press, W. H., & Schechter, P. 1974, ApJ, 187, 425
Ricotti, M., Gnedin, N. Y., & Shull, J. M. 2002a, ApJ, 575, 49
———. 2002b, ApJ, 575, 33
Ricotti, M., & Ostriker, J. P. 2004a, MNRAS, 350, 539
———. 2004b, MNRAS, 352, 547
Ricotti, M., Ostriker, J. P., & Gnedin, N. Y. 2005, MNRAS, in press (astro-ph/0404318)
Ricotti, M., & Shull, J. M. 2000, ApJ, 542, 548
Salvaterra, R., & Ferrara, A. 2003, MNRAS, 339, 973
Santos, M. R., Bromm, V., & Kamionkowski, M. 2002, MNRAS, 336, 1082
Schaerer, D. 2000, in ASP Conf. Ser. 221, Stars, Gas, and Dust in Galaxies: Exploring the Links, ed. D. Alloin, K. Olsen, & G. Galaz (San Francisco: ASP), 99
———. 2002, A&A, 382, 28
———. 2003, A&A, 397, 527
Scott, D., & Rees, M. J. 1990, MNRAS, 247, 510
Sheth, R. K., Mo, H. J., & Tormen, G. 2001, MNRAS, 323, 1
Sheth, R. K., & Tormen, G. 1999, MNRAS, 308, 119
———. 2002, MNRAS, 329, 61
Smith, L. J., Norris, R. P. F., & Crowther, P. A. 2002, MNRAS, 337, 1309
Sokasian, A., Yoshida, N., Abel, T., Hernquist, L., & Springel, V. 2004, MNRAS, 350, 47
Somerville, R. S., & Livio, M. 2003, ApJ, 593, 611
Songaila, A. 2001, ApJ, 561, L153
Songaila, A., & Cowie, L. L. 1996, AJ, 112, 335
Stanek, K. Z., et al. 2003, ApJ, 591, L17
Steidel, C. C., Pettini, M., & Adelberger, K. L. 2001, ApJ, 546, 665
Stetcher, T. P., & Williams, D. A. 1967, ApJ, 149, 29
Taylor, C. L., Hüttemeister, S., Klein, U., & Greve, A. 1999, A&A, 349, 424
Tegmark, M., Silk, J., Rees, M. J., Blanchard, A., Abel, T., & Palla, F. 1997, ApJ, 474, 1
Venn, K., Tolstoy, E., Kaufer, A., & Kudritzki, R. P. 2004, in Origin and Evolution of the Elements, ed. A. McWilliam & M. Rauch (Cambridge: Cambridge Univ. Press), 58
Vreeswijk, P. M., Møller, P., & Fynbo, J. P. U. 2003, A&A, 409, L5
Walter, F., Taylor, C. L., Hüttemeister, S., Scoville, N., & McIntyre, V. 2001, AJ, 121, 727
Whalen, D., Abel, T., & Norman, M. L. 2004, ApJ, 610, 14
Wood, K., & Loeb, A. 2000, ApJ, 545, 86
Woosley, S. E. 1993, ApJ, 405, 273
Woosley, S. E., & Weaver, T. A. 1986, ARA&A, 24, 205
York, D. G., et al. 2000, AJ, 120, 1579
Zheng, W., et al. 2003, Proc. SPIE, 4850, 1132